JACS
JOURNAL OF THE AMERICAN CHEMICAL SOCIETY

ARTICLE

pubs.acs.org/JACS

Understanding the Electronic Structure of 4d Metal Complexes: From Molecular Spinors to L-Edge Spectra of a di-Ru Catalyst

Igor Alperovich,[†,‡] Grigory Smolentsev,[§] Dooshaye Moonshiram,[†] Jonah W. Jurss,[∥] Javier J. Concepcion,[∥] Thomas J. Meyer,[∥] Alexander Soldatov,[‡] and Yulia Pushkar*[,†]

[†]Department of Physics, Purdue University, 525 Northwestern Avenue, West Lafayette, Indiana 47907, United States

[‡]Research Center for Nanoscale Structure of Matter, Southern Federal University, 5 Zorge Street, 344090, Rostov-on-Don, Russian Federation

[§]Department of Chemical Physics, Lund University, P.O. Box 124, SE-22100 Lund, Sweden

[∥]Department of Chemistry, University of North Carolina at Chapel Hill, Chapel Hill, North Carolina 27599, United States

Supporting Information

ABSTRACT: $L_{2,3}$-edge X-ray absorption spectroscopy (XAS) has demonstrated unique capabilities for the analysis of the electronic structure of di-Ru complexes such as the blue dimer *cis,cis*-$[Ru^{III}_2O(H_2O)_2(bpy)_4]^{4+}$ water oxidation catalyst. Spectra of the blue dimer and the monomeric $[Ru(NH_3)_6]^{3+}$ model complex show considerably different splitting of the Ru $L_{2,3}$ absorption edge, which reflects changes in the relative energies of the Ru 4d orbitals caused by hybridization with a bridging ligand and spin-orbit coupling effects. To aid the interpretation of spectroscopic data, we developed a new approach, which computes $L_{2,3}$-edges XAS spectra as dipole transitions between molecular spinors of 4d transition metal complexes. This allows for careful inclusion of the spin-orbit coupling effects and the hybridization of the Ru 4d and ligand orbitals. The obtained theoretical Ru $L_{2,3}$-edge spectra are in close agreement with experiment. Critically, existing single-electron methods (FEFF, FDMNES) broadly used to simulate XAS could not reproduce the experimental Ru L-edge spectra for the $[Ru(NH_3)_6]^{3+}$ model complex nor for the blue dimer, while charge transfer multiplet (CTM) calculations were not applicable due to the complexity and low symmetry of the blue dimer water oxidation catalyst. We demonstrated that L-edge spectroscopy is informative for analysis of bridging metal complexes. The developed computational approach enhances L-edge spectroscopy as a tool for analysis of the electronic structures of complexes, materials, catalysts, and reactive intermediates with 4d transition metals.

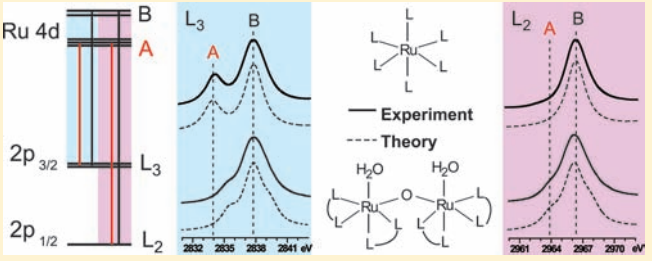

1. INTRODUCTION

X-ray absorption spectroscopy (XAS) at $L_{2,3}$-edges of transition metals (TM) reflects excitations from 2p to unoccupied levels with primary d-character. $L_{2,3}$-edge spectra provide direct information about details of the electronic structure of the metal centers in transition metal complexes, catalysts, and materials.[1−3] However, the power of this technique has been largely underutilized in studies of the electronic structure of 4d TM complexes due to complications with the theoretical treatment as well as experimental problems in obtaining spectra without artifacts. Earlier, analyses of Ru L-edges were reported for Ru-containing oxides, perovskite systems, and the $[Ru(NH_3)_6]Cl_3$, K_3RuCl_6, and $[Ru(bpy)_3]^{2+}$ model complexes.[4−8] An increasing interest in analysis of L-edge spectra is expected as new soft X-ray free electron lasers, covering the suitable energy range for this spectroscopy, are coming online. Work at Ru L-edges is motivated by the need of electronic structure analysis of Ru-based water oxidation catalysts and catalytic intermediates in the water oxidation reaction. For these catalysts, the changes in Ru oxidation state are central to the catalytic activity.[9−12] Information on the electronic structure of Ru-based catalysts for water oxidation is of great importance in facilitating our understanding of the water oxidation mechanism and in developing new, efficient catalysts for utilization in light-to-energy conversion devices for solar fuels.

A wide variety of transition metal complexes exist as multinuclear μ-oxo-bridged or, in general, ligand-bridged complexes. The electronic structures of such complexes can be quite intriguing due to various types of interactions between the metal centers facilitated by the presence of the bridging ligand. Multinuclear metal sites occur in some important metalloenzymes, but they usually contain 3d transition metals. We found only a few examples of L-edge analyses of dinuclear sites.[13,14]

To take full advantage of L-edge spectroscopy for analysis of electronic structures, in particular for molecules containing several metal centers interacting via ligands, it is desirable to have a simulation tool that can predict the $L_{2,3}$-edge XANES

Received: August 6, 2011
Published: August 25, 2011

spectra on the basis of the molecular geometry and electronic configuration of the transition metal complex. Implementation of full multiple scattering (FMS) and *ab initio* approaches within and beyond the muffin-tin (MT) potential approximation[15,16] is available in the widely used FEFF[17−19] and FDMNES[20] codes. XAS spectra of 4d transition metals are less affected by multiplet effects, which makes it possible to apply single electron approaches to describe their XAS spectra. However, we demonstrate that FEFF and FDMNES fail to reproduce the $L_{2,3}$-edge XANES spectra of the $[Ru(NH_3)_6]^{3+}$ model complex and the "blue dimer", *cis,cis*-$[Ru^{III}_2O(H_2O)_2(bpy)_4](PF_6)_4$, water oxidation catalyst, and we discuss possible reasons for the observed inconsistencies.

The charge transfer (CT) multiplet (CTM) approach developed by Thole and de Groot[21−23] (CTM4XAS code) includes charge transfer and multiplet effects. This technique successfully reproduced the L-edges spectra of $[Ru(NH_3)_6]^{3+}$, Ru-containing crystals with Ru^{IV} and Ru^{V} centers such as $Ru^{IV}O_2$, $Sr_2Ru^{IV}O_4$, and $Sr_4Ru_2{}^{V}O_9$[5], and the long-lived, lowest lying triplet exited state of the photosynthesizer $[Ru^{II}(bpy)_3]^{2+}$, $[Ru^{III}(bpy)_2(bpy^{-})]^{2+}$.[4,24] Multiplet effects with the Slater integrals reduced to 25% of their atomic values for $[Ru(NH_3)_6]^{3+}$,[23] to 40% for Ru^{IV}, and to 15% for Ru^{V} were introduced to simulate the experimental spectra.[5,25] These are large corrections because multiplet effects are considered to be small for 4d transition metals.[16] While CTM calculations were successfully used in these cases, they have limited applicability for analysis of water oxidation catalysts. The CTM4XAS code is currently limited to complexes of relatively high symmetry, while catalysts for water splitting are all low symmetry complexes. The number of adjustable parameters used in CTM calculations increases when the TM ion is located in a lower symmetry environment, which decreases the predictive performance of multiplet structures. Moreover, the percentage of Slater integral reduction is an adjustable parameter, which cannot be predicted on the basis of the molecular and electronic structures of complexes.

To overcome the limitations of the currently available simulation techniques, we introduce a new approach for simulation of Ru $L_{2,3}$-edge XANES spectra based on the two-component relativistic zeroth-order regular approximation (ZORA) implemented in the density functional theory (DFT). This approach allows direct inclusion of spin-orbit coupling effects and hybridization between Ru 4d and ligand orbitals. Theoretical Ru $L_{2,3}$-edges spectra derived with this approach are in good agreement with experiment for both monomeric and dimeric Ru complexes. The relatively small multiplet effects for the 2p−4d interaction and the efficient screening of the 2p core hole in Ru make our approach suitable for description of the Ru $L_{2,3}$-edges. We suggest that this approach should be applicable for simulations of L-edges of other 4d transition metals. Utilization of spinors is not limited to X-ray absorption and can also be used to describe X-ray emission spectra and others detecting dipole-allowed transitions.

2. MATERIALS AND METHODS

2.1. Synthesis. For XAS spectroscopy at Ru L-edges, it is important to use nonchlorinated compounds because the Cl K-edge interferes with the Ru L_3-edge. The blue dimer as the PF_6^- salt, $[((bpy)_2Ru^{III}(H_2O))_2O](PF_6)_4$, was prepared from $[((bpy)_2Ru^{III}(H_2O))_2O](ClO_4)_4$, prepared as described earlier,[26] by metathesis by adding NH_4PF_6 to an aqueous solution of the ClO_4^- salt. The dimer cation was prepurified by chromatography on LH-20 Sephadex. Purity was verified by comparison with known electrochemical and electronic spectra.[26] The salt $Ru(Mebimpy)(bpy)(H_2O)](NO_3)_2$, where Mebimpy = 2,6-bis(1-methylbenzimidazol-2-yl)pyridine and bpy = 2,2′-bipyridine, was prepared as described previously.[27]

2.2. XAS Measurements. XAS results were collected at the Advanced Photon Source (APS) at Argonne National Laboratory on beamline 9 at a photon energy of 2.3−3.0 keV and an average current of 100 mA. A Si(110) crystal monochromator with ∼0.3 eV energy resolution was used, and the intensity of the incident X-rays was monitored by a 100% filled He ion chamber (I_0) in front of the sample. XAS on the microdispersed powder samples was measured in a total electron yield mode. A thin layer of the sample was dispersed on conducting carbon film. Data on solutions were recorded as fluorescence excitation spectra using a 4-element energy-resolving detector. The solution samples were prepared by dissolving the complexes in HNO_3 solution (pH = 1) or in water at 1 mM concentration. Recorded this way, the data were free of self-absorption artifacts. The spectrum of $[Ru(NH_3)_6]^{3+}$ was similar to those reported earlier.[7,23,24,28] However, better quality was achieved here by using PF_6^- salt. The samples were kept at 80 K in a He atmosphere at ambient pressure using a continuous-flow liquid N_2 cryostage. To reduce the sample damage by X-ray, 80% flux was used, and no damage was observed in consecutive scans. No more than five scans were taken at each sample position.

The Ru XAS energy was calibrated by the maxima of the L_3-edge of ruthenium metal (2838 eV), which was measured in the sample position twice a day during the beamtimes (no variation between the calibrations was detected from day to day during each single beamtime). The XAS data were recorded during three beamtimes.

2.3. XAS Calculations. *FEFF9.05.* FEFF spectra were simulated by using the self-consistent FMS code FEFF9.05.[17−19] The Hedin−Lundqvist exchange-correlation (XC) potential with time-dependent local density approximation (TDLDA) was employed. It accounts for a dynamic screening of the X-ray and the core-hole fields[17] and is said to improve the agreement for experimental transition metal (TM) $L_{2,3}$-edges spectra and the intensity ratio of the L_2/L_3-edges in particular. We have also tried other options such as various XC potentials, adding extra charge, and attempting a multitude of core-hole treatments; however, no significant effects on the spectra shape were observed (Figure S1). Default values were used for all other parameters.

FDMNES2010. The *ab initio* FDMNES spectral calculation is based on the Schrödinger equation, solved using the finite difference method with the free potential shape having a Hedin−Lundqvist exchange-correlation component. The initially obtained discrete spectra were then broadened within the arctangent-dependent width model to take into account the finite mean free path of the photoelectron, the core-hole lifetime (1.92 eV for L_2-edge[29] and 1.75 eV for L_3-edge),[30,31] and the energy resolution of the monochromator (∼0.3 eV). Theoretical simulations of XANES spectra of the blue dimer with the FDMNES2010 code are computer resource intensive due to the large size of the molecule and the absence of symmetry. Therefore, we performed the FDMNES simulations without MT potential approximation for 52 atomic clusters (5.1 Å radius around the absorber), which should be quite sufficient and considerably better than the 19-atomic cluster FDMNES calculations reported earlier.[15]

2.4. Molecular Structures. The geometry of the $[Ru(NH_3)_6]^{3+}$ model complex was assumed to be of high D_{3d} symmetry with Ru−N distances being constrained to 2.1 Å (distance determined from EXAFS).[7] The blue dimer Ru_1^{III}, Ru_2^{III} (hereafter abbreviated [3,3]) coordinates were obtained from X-ray diffraction data.[26]

2.5. Modeling of the Ru $L_{2,3}$ XAS Spectra Based on DFT Calculations. Here, we developed an approach for simulation of Ru $L_{2,3}$-edges based on the relativistic two-component zeroth-order regular approximation (ZORA) DFT calculations. We used as the basis

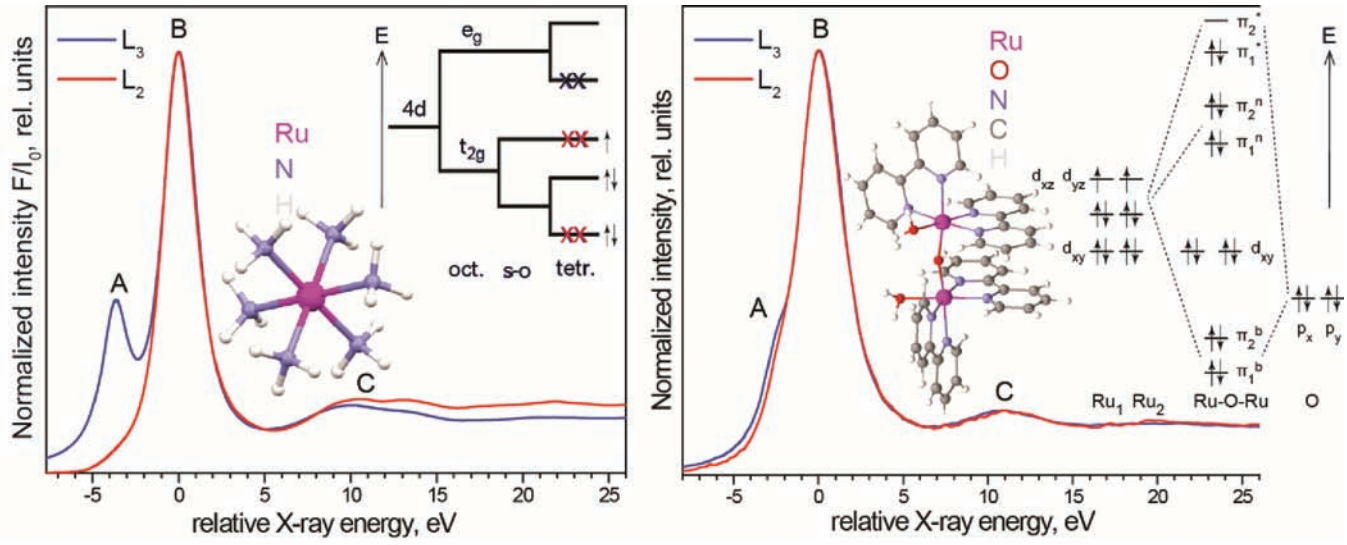

Figure 1. (A) Experimental Ru $L_{2,3}$-edges XANES spectra of $[Ru(NH_3)_6](PF_6)_3$. A relative energy scale is used with 0 corresponding to 2840.1 eV for L_3- and 2968.9 for L_2-edges, and the spectral intensity was adjusted for easy comparison. The inset shows a schematic energy diagram of the 4d orbitals as they successively experience an octahedral field, a spin-orbit splitting, and a weak tetragonal distortion. Electrons occupying orbitals are denoted by arrows. The presence of vacant orbitals in both the t_{2g} and the e_g manifolds for Ru^{3+} (d^5) allows detection of transitions from the 2p level to both the t_{2g} and the e_g set of levels, denoted by the A and B peaks. Thus, A/B splitting can be used to estimate 10Dq, the crystal field splitting parameter.[7] The forbidden transitions at the L_3-edge are marked (XX-black), and both (XX-black and XX-red) are forbidden transitions at the L_2-edge. (B) Experimental Ru $L_{2,3}$-edges XANES spectra of BD [3,3]. A relative energy scale is used with 0 corresponding to 2840.1 eV for L_3- and 2968.9 for L_2-edges, and the spectral intensity was adjusted for easy comparison. The inset shows molecular orbitals involving the Ru 4d electrons in the blue dimer at the closed-shell electronic state.

Slater orbitals as implemented in the ADF2010 package.[32,33] Molecular structures of Ru-complexes were used as inputs. The $[Ru(NH_3)_6]^{3+}$ complex has a d^5 configuration so it is an open-shell molecule. The blue dimer (BD) [3,3] compound has closely spaced singlet and triplet spin states. Thus, we have chosen to do spin-unrestricted calculations (needed to describe open shell molecules). Such calculations result in molecular orbitals (MOs) that are two-component spinors (1) and, thus, contain wave functions associated with both spin up and spin down states:

$$\psi_j^{\mathrm{MO}} = \begin{pmatrix} \psi_\alpha \\ \psi_\beta \end{pmatrix} = \begin{pmatrix} \psi_\alpha^{\mathrm{Re}} + i\psi_\alpha^{\mathrm{Im}} \\ \psi_\beta^{\mathrm{Re}} + i\psi_\beta^{\mathrm{Im}} \end{pmatrix} \quad (1)$$

Intensities of 2p-to-unoccupied states XAS transitions were calculated by integration of dipole transition matrix elements between 2p-originated MOs (Ψ_{2p_k}) and unoccupied MOs, denoted as Ψ_j:

$$I_{\mathrm{Ru}\ 2p_k \rightarrow \mathrm{LUMO}\ j} \sim |\langle \psi_j | \hat{\mu} | \psi_{2p_k} \rangle|^2$$
$$k = 1...6;\ j = \mathrm{LUMO}...\mathrm{LUMO} + N \quad (2)$$

where Ψ_{2p_k} and Ψ_j are the initial and final states spinors, respectively; index k enumerates six MOs that comprise the Ru 2p-atomic orbitals from which Ru $L_{2,3}$ XAS excitations are calculated; and $\hat{\mu}$ is the dipole transition matrix operator. This method allows us to account for spin-orbit coupling effects. In DFT calculations for each spinor (1), four numerical values of its components' were extracted on a 3D spatial grid in close proximity to the absorbing ruthenium atom. While the electronic density of the Ψ_{2p_k} atomic-like MOs is localized near the Ru atom (Figures S2,S3), unoccupied MOs can be delocalized. Because only integration over the area where Ψ_{2p_k} is nonzero will result in a contribution to integrals like (2), we demonstrate that integration over a 3D cubic grid centered on the absorber with a 0.46 Å edge is sufficient to cover the area containing more than 99% of Ψ_{2p_k} electron density (Figure S4). Thus, we restricted the integration domain of (2) to this region. Additional tests demonstrated that we achieved grid-size convergence, and further expansion of the integration range does not result in any noticeable spectral changes (Figure S5). Simulation of the XANES spectral region including peaks A, B, and C (Figure 1) requires integration (2) for the lowest few hundreds of unoccupied MOs. Finally, Lorentzian broadening of this discrete spectrum was performed using the energy-dependent arctangent model. This accounted for the finite mean free path of the photoelectron, the core hole lifetime broadening (~2 eV), and the monochromator resolution (~0.3 eV) (see the Supporting Information and Figure S6).

For DFT calculations, we tested several combinations of exchange-correlation potentials with basis sets of Slater-type orbitals of various sizes (Table 1). The following exchange correlation (XC) potentials[34] were used: local density approximation (LDA) with parametrization by Vosko, Wilk, and Nusair,[35] generalized gradient approximation with Perdew–Wang XC part (GGA:BP),[36,37] together with asymptotically correct LB94[34] and the statistical average of orbital potentials (SAOP).[38,39] For $[Ru(NH_3)_6]^{3+}$, double-ζ, triple-ζ, and quadruple-ζ basis sets of Slater-type were used. For the blue dimer molecule, only the triple-ζ basis set was used.

3. RESULTS AND DISCUSSION

3.1. Electronic Structures of the Monomeric $[Ru(NH_3)_6]^{3+}$ and di-Ru "Blue Dimer" Complexes and Their Manifestation in $L_{2,3}$-Edge Spectra. The absorption edge of Ru L_2- and L_3-edges XANES mainly reflect electron transitions from the Ru core $2p_{1/2}$ and $2p_{3/2}$ to the unoccupied 4d orbitals. Thus, it contains direct information about the arrangement of unoccupied molecular orbitals (MOs) with high contribution of Ru 4d electrons. The inset in Figure 1A shows a schematic energy

Table 1. List of Correlation Potentials and Basis Sets That Were Used in Spectra Simulations by DFT-Based Approach

	Slater-type orbitals		
method[a]	XC potential	basis set	A/B splitting, eV
	$[Ru(NH_3)_6]^{3+}$		
experiment			3.70
1	LDA	DZ	4.10
2	LDA	TZP	4.05
3	LDA	QZ4P	4.02
4	GGA:BP	QZ4P	3.78
5	LB94	TZP	3.87
6	LB94	QZ4P	3.87
7	SAOP	QZ4P	3.78
	$[Rh(NH_3)_6]^{3+}$		
8	LDA	QZ4P	4.41
	BD [3,3]		
experiment			2.30
	BD [3,3]with Spin-Orbit Coupling		
9	LDA	TZP	2.39
10	GGA:BP	TZP	2.28
11	LB94	TZP	2.28
12	SAOP	TZP	2.48
13	SAOP	DZ	2.34
	BD [3,3] without Spin-Orbit Coupling		
1 singlet	LB94	TZP	2.43
2 triplet	LB94	TZP	2.26
3 singlet	SAOP	TZP	3.26
4 triplet	SAOP	TZP	2.77

[a] Calculations 1−13 were done with the two-component ZORA relativistic approximation.

diagram of the 4d orbitals in the monomeric Ru complex as they successively experience an octahedral field, a spin-orbit splitting, and a weak tetragonal distortion. The presence of vacant orbitals in both the t_{2g} and the e_g manifolds for Ru^{3+} (d^5) allows detection of transitions from the 2p level to both the t_{2g} and the e_g set of levels, denoted by the A and B peaks. Thus, A/B splitting can be used to estimate 10Dq, the crystal field splitting parameter. Transitions to the t_{2g} level are not observed at Ru L_2-edge due to spin-orbit effects (Figure 1A). To explain the Ru L-edge absorption spectrum in the $[Ru(NH_3)_6]Cl_3$ model complex salt, Sham explicitly calculated the dipole transition intensities between $2p_{j,mj}$ and the unoccupied valence levels with 4d character.[7] He demonstrated that the dipole transition to the empty t_{2g} state can only arise from the $p_{3/2}$ electrons, explaining the absence of peak A for the L_2-edge (transitions from $2p_{1/2}$ to unoccupied MOs) (Figure 1A). The symmetry argument can help to understand the observed phenomenon if one considers that 4d spin-orbit coupling removes the degeneracy of both the $^2T_2$ atomic ground and the $^2T_1$ final states,[4] thus making the dipole transition of the $2p_{1/2}$ core level electron to the t_{2g}-related orbital forbidden (Figure 1A, inset). Therefore, peak A at the L_2-edge disappears completely in the case of a Ru^{3+} XAS for O_h symmetry compounds.

When two Ru^{3+} (d^5) ions are located in one molecule with a bridging ligand, the frontier molecular orbitals are built by the 10 electrons contributed by the two Ru^{3+} (d^5) centers, each of which finds itself in a pseudo-octahedral environment. With the Ru−Ru axis denoted by z, this geometry leads to a natural splitting between the σ (d_{x2-y2}, d_{z2}), π (d_{xz},d_{yz}), and δ (d_{xy}) orbitals. On the basis of a series of experiments, Weaver et al.[9] proposed the MO diagram for the "blue dimer" shown in Figure 1B. The lowest two orbitals are bonding and principally O(2p) in character. A pair of nonbonding (or weakly bonding) δ (d_{xy}) orbitals arise from the d manifold, followed by the in-phase combinations of the (d_{xz},d_{yz}) orbitals (π_1, π_2) and finally the antibonding combination (π_1^*, π_2^*). Three candidates for the ground state were discussed by Weaver et al.: the closed-shell $[\delta^4\pi_1^2\pi_2^2\pi_1^{*2}]$ strong coupling configuration, the triplet state $[\delta^4\pi_1^2\pi_2^2\pi_1^*\pi_2^*]$, and a weak coupling valence bond-like singlet arising from coupling of localized $S = 1/2$ Ru centers. The analysis in Figure 1B suggests that the arrangement of unoccupied orbitals in the "blue dimer" should be considerably different from those in monomeric Ru complexes. The bridging ligand, in this case oxygen, contributes considerably to LUMO, shifting its energy as compared to monomeric complexes. The Ru $L_{2,3}$-edges for the "blue dimer", *cis,cis*-$[Ru^{III}_2O(H_2O)_2(bpy)_4](PF_6)_4$, in its initial oxidation state [3,3] (Figure 1B) show considerably different splitting of the A/B peaks as compared to the monomeric Ru complex. This observation confirms the suggested changes in the relative energies of the unoccupied orbitals with predominantly d-character.

A closer look at the L_2 spectrum of BD [3,3] (Figure 1B) shows that, contrary to $[Ru(NH_3)_6]^{3+}$, there is a small shoulder A in the L_2-edge spectrum. This difference can be readily explained by the low symmetry at the Ru center in BD [3,3]. This was also observed in the L_2-edge of transient species $[Ru^{III}(bpy)_2(bpy^-)]^{2+}$.[4] Following the arguments of Gawelda et al.,[4] one can demonstrate that trigonal distortion mixes the spin-orbit split states in the initial ($2p^64d^5$) state. Transitions from one of these ground states are allowed for all symmetries, and mixing makes more transitions allowed resulting in the shoulder A in the L_2-edge. Thus, for BD [3,3], feature A is present at both edges. A careful comparison of the BD [3,3] L_3- and L_2-edges spectra show that they are not exactly identical (Figure 1B). The shoulder A is less pronounced in the L_2-edge spectrum.

In addition to this, $L_{2,3}$-edge spectra contain information about the oxidation state of the Ru centers. To extract this information, it is important to compare the Ru $L_{2,3}$-edges of BD [3,3] and other model compounds with Ru in oxidation state Ru(II) ($[Ru(Mebimpy)(bpy)(H_2O)]^{2+}$) and Ru(III) ($[Ru(NH_3)_6]^{3+}$) (Figure 2). Spectra of other monomeric Ru(II) and Ru(III) complexes were recorded, but they were very similar to those displayed and are therefore not shown. Figure 2 demonstrates a considerable shift of the $L_{2,3}$-edges of BD [3,3] and $[Ru(NH_3)_6]^{3+}$ as compared to the complex $[Ru(Mebimpy)(bpy)(H_2O)]^{2+}$. However, the positions of peak B in BD [3,3] and $[Ru(NH_3)_6]^{3+}$ are almost identical at the L_3-edge, and the apparent shift in BD [3,3] relative to $[Ru(NH_3)_6]^{3+}$ at the L_2-edge is due to an increase in the number of allowed transitions in BD (see below). Our data support the assignment of the oxidation states of the Ru centers in BD [3,3] to Ru^{III}.

To go from the descriptive comparison above to a quantitative analysis, we need to simulate Ru $L_{2,3}$-edges spectra. Because of the high complexity of the "blue dimer" molecule, we first evaluated various simulation approaches for the model $[Ru(NH_3)_6]^{3+}$ complex.

3.2. Evaluation of the Existing Single-Electron Theoretical Approaches for Simulation of the Ru $L_{2,3}$-Edges in the

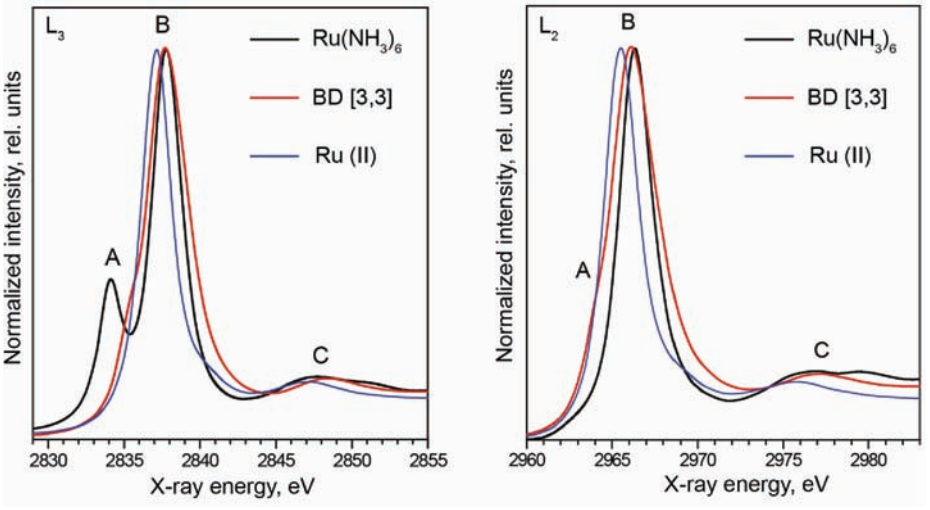

Figure 2. Comparison of the blue dimer [3,3] and $[Ru(Mebimpy)(bpy)(H_2O)]^{2+}$ (denoted Ru(II)), $[Ru(NH_3)_6]^{3+}$ reference compounds. (Left panel) Ru L_3-edge spectra; (right panel) Ru L_2-edge spectra.

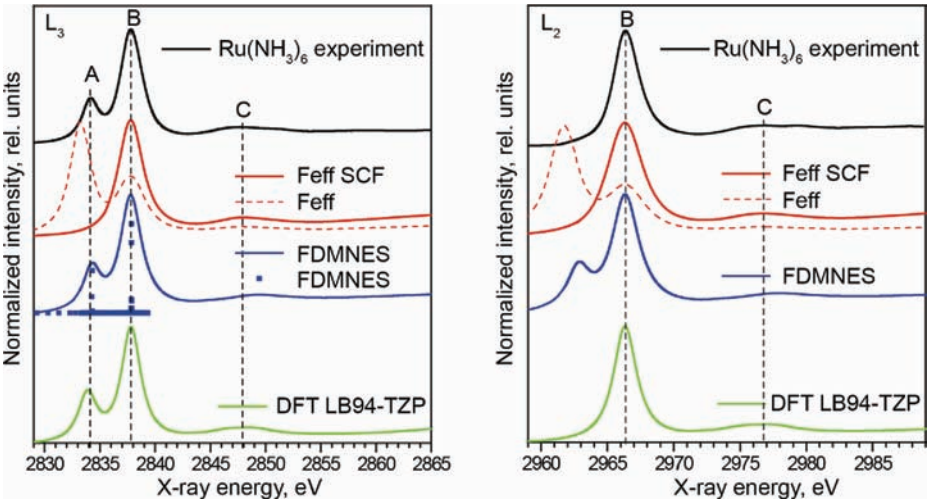

Figure 3. L_3-edges (left panel) and L_2-edges (right panel): experimental spectra of $[Ru(NH_3)_6]^{3+}$ (black); calculations with FEFF code with *E* Fermi (E_f) determined by FEFF self-consistently (red line) or manually adjusted to −6 eV from value determined by FEFF (dashed red line); calculations with FDMNES code (blue line). Unbroadened FDMNES spectrum (blue ■) is shown for splitting of the white line (A/B splitting); calculations with DFT approach with LB94 exchange correlation potential and triple-ζ (TZP) basis set (green lines). Neither FEFF nor FDMNES reproduces differences between L_3- and L_2-edges observed experimentally. DFT approach reproduces experimental spectra very well.

$[Ru(NH_3)_6]^{3+}$ Model Complex. While it was vigorously demonstrated that single-electron codes perform poorly for simulations of 3d transition metal $L_{2,3}$-edges,[16] their applicability to 4d metal ions is under debate. The relatively small multiplet effects for the 2p core levels of the 4d metal imply that one-electron codes can be used as a first approximation.[12] Among the single electron techniques, FMS calculations seem to be an attractive approach for simulation of the Ru $L_{2,3}$ XAS. They satisfy some of our criteria such as: (1) use of molecular structure of the Ru complex as an input, and (2) ability to deliver spectra in a wide energy range. The Ru L-edges display spectral features above the absorption edge (peak C, Figure 1), which potentially carry information about the structure of Ru complexes. In Benfatto et al., the spectra of $[Ru^{II}(bpy)_3]^{2+}$ and $[Ru^{III}(bpy)_2(bpy^-)]^{2+}$ calculated with the FMS approach demonstrated some features of the experimental spectra,[15,24] but failed to give a good agreement with experiment. Nevertheless, it was not clear to us to what extent it can reproduce details of the splitting in the absorption edge. Figure 3 shows a comparison of the experimental Ru $L_{2,3}$-edges for the $[Ru(NH_3)_6]^{3+}$ model complex (black line) and calculations with FEFF9.05 code based on FMS approach with muffin-tin potential approximation (red lines). When the Fermi level (E_F) is obtained by FEFF using its self-consistent approach, only one peak is present in L_3 and L_2 spectra (red line, Figure 3). This disagrees with experimental data for the L_3-edge. When E_F is manually set to be red-shifted by −6 eV as compared to E_{Fermi} determined by FEFF, a second peak can be observed with an intensity larger than that of peak B (red dash line, Figure 3). Manual adjustment of the E_f shift to some value between −6 and 0 eV can potentially result in an A/B ratio close to that observed in the experimental L_3 spectrum. However, such an exercise has very little meaning when one wants to predict the experimental

spectrum for a particular molecular complex. Figure 3 shows that the FEFF calculation overestimates $t_{2g}-e_g$ splitting (splitting between A and B peaks). The described discrepancies persist despite inclusion of several additional options (see Materials and Methods) claimed to be productive[17] in other TM $L_{2,3}$ XANES simulations. Other parameter settings were also tested with no important differences being observed (Figure S1). It is important to emphasize that FEFF cannot reproduce the experimentally observed difference between the L_3- and L_2-edges.

Use of the *ab initio* finite-difference method (FDM) to solve the Schrödinger equation results in a modest improvement (blue line, Figure 3). Here, the calculated splitting of the $t_{2g}-e_g$ manifold (A/B splitting) and the relative intensities of the A/B peaks in the L_3-edge are in better agreement with experiment. However, the differences between the L_3- and L_2-edges still cannot be reproduced.

Looking for a possible origin of the discrepancies between the predictions of FMS and FDM codes and experimental spectra, we can mention that those codes are mainly optimized for calculations in the continuum part of the energy spectrum. Complex potentials or integration in the complex energy plane are used in the FMS theory to address discrete states. Numerical algorithms of the FDM and FMS techniques might effectively broaden discrete peaks. In case this broadening is larger than the spin-orbit splitting of energy levels, it may have a range of consequences, such as complications in resolving occupied states from unoccupied (problems to find the right Fermi level) or apparent insensitivity to selection rules. This can lead to incorrect predictions of L_2- and L_3-edge spectra. From personal communication with the developer of the FDMNES code, Dr. Joly, we have learned that implementation of spin-orbit coupling treatment is still under development in this code.

The above analysis demonstrates that results of the single electron approaches with MT and beyond MT potential approximation have to be taken with extreme caution as they may fail to correctly describe splitting of peaks and their relative intensities at the absorption edge. In the $[Ru(NH_3)_6]^{3+}$ model complex, these approaches cannot reproduce differences between L_2- and L_3-edges.

3.3. DFT-Based Analysis of the Ru $L_{2,3}$-Edges XANES for $[Ru(NH_3)_6]^{3+}$. The obvious limitations of the currently available FMS, FDM, and multiplet approaches prompted us to look for our own solution to the problem. Below, we evaluate an approach for calculation of the XANES spectra based on ground-state DFT calculations with the two-component ZORA relativistic approximation. We had to limit ourselves to ground-state calculations as time-dependent (TD) DFT at this level of theory is currently not possible for open-shell systems.[40] In our approach, the geometry of the molecule is used as an input. MOs are derived in calculations that take into account all electrons of the Ru center contrary to more common use of frozen-core potential for Ru. XAS intensities are calculated numerically by integration of dipole transition matrix elements between the Ru 2p core-levels and the unoccupied valence band MOs (see Materials and Methods). The main advantage of this approach is a correct inclusion of spin-orbit coupling effects. Combinations of basis sets and exchange correlation potentials were tested for the $[Ru(NH_3)_6]^{3+}$ molecule (Table 1, Figure S7). For various basis sets and exchange correlation potentials (Table 1), we found the splitting of the Ru 2p level to vary from 126 to 133 eV, which is close to the experimental value of 128.8 eV. The relative intensities of peaks A/B are unaffected by the selection of basis set/potential, and the A/B splitting changes very little as indicated in Table 1. All tested combinations of exchange potentials and basis sets resulted in spectra that are close to experiment and reproduce the differences between the L_3- and L_2-edges well. An example is given in Figure 3.

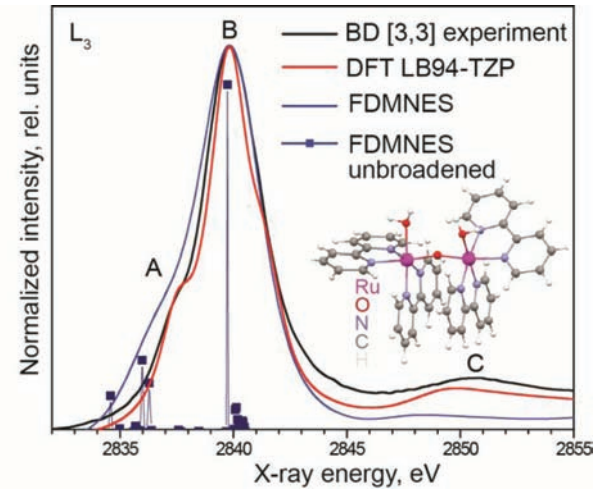

Figure 4. Comparison of the experimental Ru L_3-edge spectrum of BD [3,3] complex (black) and calculations using FDMNES code (blue) and DFT-based approach developed here (red). Unbroadened spectrum (blue line with ■) is shown for splitting of the white line (A/B splitting) from FDMNES calculations.

DFT calculations result in a set of discrete transitions. However, somewhere above the absorption edge the discrete spectrum will change to a continuum and, thus, should not be described by DFT. One way to estimate the limits of validity of the DFT approach is to obtain the ionization potential by peak fitting analysis of the experimental spectra (Figure S8, Table S1). The analysis in Figure S8 shows that IP lies just below peak C. This peak can be understood as transitions to quasi bound states (see discussion below). Interestingly, DFT predicts the presence of this peak, and use of larger basis sets improves its position (Figure S7). We note that use of double-ζ basis sets of Slater-type orbitals is insufficient for description of spectral feature past white line, while use of triple-ζ and quadruple-ζ gives similar results (Figure S7). Among the three tested correlation potentials, LB94 provides the best match with experimentally observed spectra (Figure S7). Both LDA and SAOP potentials result in additional features between peaks B and C in the L_2- and L_3-edges, which are not detected experimentally. They also show a small shoulder on the L_2-edge, which is not observed in the experiment.

In L-edge XANES, electron excitation results in a hole at the 2p level. Various approaches are possible for its treatment such as $Z+1$ approximation[41] or dynamical screening models.[42] Spectra computed for the $[Rh(NH_3)_6]^{4+}$ complex ($Z+1$ approximation) are similar to those of $[Ru(NH_3)_6]^{3+}$; however, they show less agreement with experiment (Figures S9,S10). Overall, we attribute the surprisingly good agreement between experiment and theory utilizing ground-state unoccupied levels to the efficient screening of the 2p hole in the heavy Ru atom and its small effects on the relative arrangement of unoccupied orbitals. Similarly, ground-state calculations (ignoring the core-hole) resulted in better agreement with experiment in other systems.[43,44]

3.4. Simulation of the Blue Dimer $L_{2,3}$ XAS. XAS spectral analysis at the Ru $L_{2,3}$-edges shows that the considerably smaller

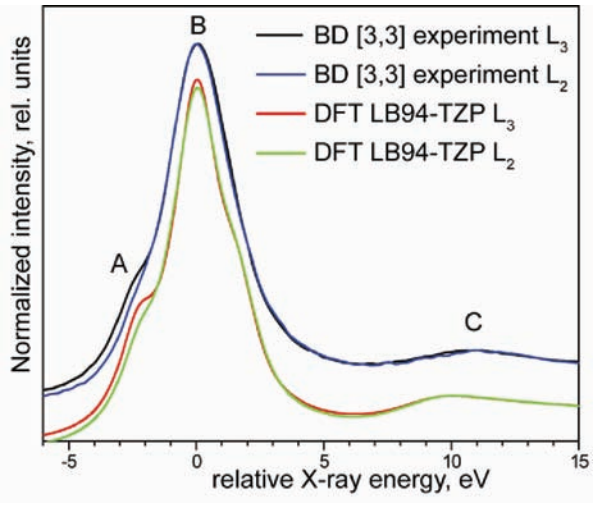

Figure 5. The comparison of the experimental and calculated Ru $L_{2,3}$-edges for BD [3,3]. Relative energy scale is used with 0 corresponding to 2840.1 eV for L_3- and 2968.9 for L_2-edges, and spectral intensity was adjusted for easy comparison. Calculations with direct inclusion of spin−orbit coupling result in close agreement with experiment.

splitting of the A/B peaks is the main difference between the "blue dimer" and monomeric Ru complexes: $[Ru(NH_3)_6]^{3+}$ (Figures 1A, 2) and $[Ru^{III}(bpy)_2(bpy^-)]^{2+}$.[4] It is critical to determine whether single electron approaches or DFT techniques can reproduce the significant decrease in A/B splitting detected experimentally for BD.

Figure 4 shows a comparison of the BD [3,3] experimental L_3 spectrum with spectra calculated with FDMNES code. This technique was selected because it reproduced the A/B splitting in $[Ru(NH_3)_6]^{3+}$ well (Figure 3). Obviously, FDMNES failed to reproduce the trend of the much smaller A/B splitting observed in the BD molecule (Figure 4). Figure 4 includes an unbroadened spectrum predicted by FDMNES. It shows that the A/B splitting determined with FDMNES for BD [3,3] is close to that of $[Ru(NH_3)_6]^{3+}$(about 3.5−4 eV) and is far from the 2.3 eV observed experimentally for the BD molecule. The reason for this large discrepancy is unknown. FDMNES simulations for the BD L_2-edge are not shown because we demonstrated earlier for the model compound that, currently, this method cannot describe differences between Ru L_3- and L_2-edges.

Figures 4 and 5 compare BD [3,3] experimental spectra and calculated XANES spectra using the DFT-based approach developed here with the two-component ZORA relativistic approximation. All tested correlation potentials (Table 1) resulted in a good description of a major decrease in A/B splitting and overall close agreement between computed and experimental spectra. For BD calculations, triple-ζ (TZP) basis set was used to deliver sufficient accuracy, while quadruple-ζ (QZP) turned out to be computationally too expensive for this molecule. All details of the spectra such as the small shoulder A in the L_2-edge spectrum and the relative differences between the L_3 and L_2 spectra of "blue dimer" are well reproduced (Figure 5). These fine details are due to some transitions at the L_2-edge, which remain forbidden or have decreased intensities. To the best of our knowledge, no other simulation approach can provide analysis of the presented experimental data at a similar level of agreement between theory and experiment. Potentially, relativistic TD-DFT could be an even better technique for this type of analysis. However, recent developments in relativistic TD-DFT are still limited to very small molecules or molecules with a closed shell.[45,46] Our approach does not account for multiplet effects. Their inclusion may result in even better agreement with experiment. A configuration interaction (CI) approach has been proposed to directly account for multiplet effects. Currently, its implementation has been demonstrated for very small molecules of high symmetry.[47] A combination of relativistic DFT and CI calculations, termed the "*ab initio* CTM" method, was recently applied to simulate XANES $L_{2,3}$-spectra of some 3d TM oxides.[48] Advantages in comparison with the CTM approach are clear. Nevertheless, some shortcomings of the CI method remained, such as high computational demands, applicability primarily to relatively small clusters of high symmetry, and absence of solid-state effects. The approach presented here is similar to "*ab initio* CTM",[48] in the sense that the effects of Ru−ligand hybridization and covalency are taken into consideration by utilization of molecular spinors.

3.5. Electronic Structure of the Blue Dimer. Here, we experimentally detected and computationally reproduced Ru $L_{2,3}$-edges spectra of the blue dimer molecule. Direct inclusion of spin-orbit coupling allows us to accurately predict spectra consistent with experiment of both the model $[Ru(NH_3)_6]^{3+}$ complex and the BD molecule. The question is whether these results can help us to better understand the interesting properties of the blue dimer, which has been studied extensively by various experimental and computational techniques. BD [3,3] is EPR silent; however, magnetic susceptibility measurements reveal 1.60 μB moment per molecule, and its solution NMR shows paramagnetic broadening. Thirty years after the discovery of this first molecular catalyst for water oxidation, the details of its electronic structure and the mechanism of catalytic activity are still being debated.[12,49,50] Interaction of two unpaired electrons of Ru centers across the μ-oxo bridge can potentially result in various spin states: a strongly coupled singlet, or an antiferromagnetically coupled singlet or triplet.[12,49,50] Because of a rather small difference in energies of the singlet and triplet states for this molecule (0.5 kcal/mol), current computational techniques have difficulty interrogating the relative energies of various spin states in this molecule.[12,49,50]

Spin-orbit coupling effects are increasingly important for heavier elements. Here, we cannot describe experimental spectra as satisfactory unless we carefully account for spin-orbit coupling. The value of spin-orbit coupling splitting of the 4d level in the Ru atom is about 0.13−0.14 eV according to different sources.[3,51] This is quite large in comparison with the small energy difference between singlet and triplet spin states in the BD molecule. We hypothesize that in this molecule spin-orbit coupling results in mixing of various spin states, mainly singlet and triplet. Because of such mixing, a pure spin state of the molecule might not be defined. Interestingly, peak A in the Ru L_3- and L_2-edges of BD contains two transitions when the molecule is described with relativistic ZORA approximation (the spin state is not defined) and for the triplet state defined with conventional DFT; however, only one transition is predicted for a strongly coupled singlet. The experimental difference in peak A/B splitting in the L_2 and L_3 spectra (Tables 1, S1) is more consistent with a triplet or spin-orbit mixed state than with a strongly coupled singlet. If only one transition is possible, a decrease in the intensity rather than a shift in energy is expected when this transition becomes partially forbidden. However, small multiplet effects also cannot be excluded.

We attempted calculations for BD in two spin states: strongly coupled singlet ($S = 0$) and triplet ($S = 1$) by doing calculations without spin-orbit coupling. In this case, it is not possible to distinguish between L_2- and L_3-edges. Therefore, we computed the combined L_{2-3} spectrum by adding transitions from the p_x, p_y, and p_z orbitals to unoccupied MOs. Figure S11 shows a comparison of spectra calculated for the singlet and triplet with the experimental spectrum and a calculation with spin-orbit coupling. A comparison of A/B splitting (Figure S11 and Tables 1, S1) for these four cases shows that the spectrum computed with spin-orbit coupling and the triplet spectrum are closer to experiments, while the corresponding singlet spectrum shows a more pronounced shoulder at peak A and larger A/B splitting. Interestingly, the relative energy levels of the lowest unoccupied orbitals for ZORA calculation are very similar to the results of calculations with conventional DFT for the triplet state (Figure S11, inset).

3.6. States above the White Line of Ru L-Edge. Ru L_2 and L_3 spectra of the model complex $[Ru(NH_3)_6]^{3+}$ and BD display peak C lying about 10 eV above the edge (Figures 1−5). Its nature generated some discussion in the past. Peak C was originally attributed to a 2p-to-5s transition.[7,24,28] Later,[4,15] it was noted that peak C lies above the ionization potential and is absent in FDMNES simulations with a small molecular cluster, 7 atoms as opposed to 19 atoms. It was then assigned to a multiple scattering (MS) resonance, which originated from scattering of a low energy outgoing photoelectron.[15] Our data show that peak C is indeed located above IP for both $[Ru(NH_3)_6]^{3+}$ and BD (Figure S8 and Table S1). However, even the smallest Ru-containing complex $[Ru(NH_3)_6]^{3+}$ demonstrated a noticeable peak C in both the experimental and the theoretical spectra (Figures 1, 2). So for this Ru complex, it is not necessary to have higher coordination spheres to generate peak C. All types of tested here calculations (FEFF, FDMNES, DFT-ZORA) reproduced the appearance of this peak for both molecules. We propose that it originates from transitions to quasi-bound states lying above the ionization potential.[52] Such transitions are well described for small diatomic molecules.[52] We noticed that the position of peak C shifts toward higher energy in the sequence: $[Ru(Mebimpy)(bpy)(H_2O)]^{2+}$, $[Ru(NH_3)_6]^{3+}$, and $[((bpy)_2Ru(H_2O))_2O]^{4+}$ (Figure 2). In this sequence, the positive charge of the complex increases, which could raise the energy of a 2p-electron to the quasi-bound state transition. The DFT-ZORA approach gives the position of peak C for $[Ru(NH_3)_6]^{3+}$ in agreement with experiment and slightly underestimates it for BD [3,3]. In the $Z+1$ approximation, peak C is shifted to higher energy (Figures S9,S10). Thus, again, we can see that the charge on the Ru complex affects the position of peak C.

4. CONCLUSIONS

The sensitivity of $L_{2,3}$-edges X-ray absorption near edge structure (XANES) spectra to the details of the electronic configuration of Ru complexes was demonstrated for the di-Ru complex *cis*,*cis*-$[Ru^{III}_2O(H_2O)_2(bpy)_4](PF_6)_4$ water oxidation catalyst. The obtained spectra are in agreement with assignment of the Ru^{III} oxidation state, however, with considerably different splitting of the Ru $L_{2,3}$ white lines as compared to monomeric Ru complexes. Existing single-electron methods (FEFF, FDMNES) cannot reproduce the details of the experimental Ru L-edge spectra for the $[Ru(NH_3)_6]^{3+}$ model complex nor for the blue dimer. With a theoretical approach using a two-component relativistic approximation, we achieved a good description of the experimentally detected electronic transitions at the Ru $L_{2,3}$-edges for the Ru model complex and the water oxidation catalyst. Our approach uses the molecular and electronic structure of the metal complex as an input for calculations and, thus, allows us to model how changes in geometry and electronic state of the catalyst will affect $L_{2,3}$-edges XAS. Our analysis of the blue dimer molecule allowed us to put forward a hypothesis that spin-orbit coupling mixes the singlet and triplet spin states in this molecule. Future experimental and theoretical characterization of the $L_{2,3}$ XAS and XES of the blue dimer catalyst with the Ru centers in high oxidation states will help to better understand the mechanism of water oxidation by this unique catalyst. Our computation techniques, with careful inclusion of spin-orbit coupling, further develop $L_{2,3}$-edges XAS as a critical tool for detailed analysis of the mechanisms of catalytic reactions in 4d transition metal complexes.

■ ASSOCIATED CONTENT

Supporting Information. Additional analysis of the experimental Ru L_3 XANES spectra, calculation details, and description of the computational DFT-based approach for Ru $L_{2,3}$-edges spectra simulations. This material is available free of charge via the Internet at http://pubs.acs.org.

■ AUTHOR INFORMATION

Corresponding Author
ypushkar@purdue.edu

■ ACKNOWLEDGMENT

Synchrotron facilities were provided by APS, Argonne operated by DOE, Office of Basic Energy Sciences, under contract W-31-109-ENG-38. We thank Dr. Trudy Bolin for help with the experiments at the Beamline BM-9, APS. D.M. was partially supported by a Purdue Research Foundation grant. We thank the U.S. Department of Energy, Office of Basic Energy Sciences, for financial support of this work under Grant nos. DE-FG02-10ER16184 (YP) and DE-FG02-06ER15788 (T.M.). Synthesis and characterization (J.J.C.) were supported by the UNC EFRC: Solar Fuels and Next Generation Photovoltaics, an Energy Frontier Research Center funded by the U.S. Department of Energy, Office of Science, Office of Basic Energy Sciences under Award Number DE-SC0001011. The work of G.S. is supported by ERC Advanced investigator grant to V. Sundstrom: VISCHEM 226136. Calculations were done with supercomputer funded by Southern Federal University (Russia). We acknowledge our communication with the developers of the FEFF (Dr. J. Rehr) and FDMNES (Dr. Y. Joly) codes. We also thank Profs. Lyudmila Slipchenko, David McMillin, Leonid Rokhinson, and Steve Durbin of Purdue University for helpful discussion.

■ REFERENCES

(1) Fink, J.; Mullerheinzerling, T.; Scheerer, B.; Speier, W.; Hillebrecht, F. U.; Fuggle, J. C.; Zaanen, J.; Sawatzky, G. A. *Phys. Rev. B* **1985**, *32*, 4899.
(2) Zaanen, J.; Sawatzky, G. A.; Fink, J.; Speier, W.; Fuggle, J. C. *Phys. Rev. B* **1985**, *32*, 4905.
(3) Groot, F. d.; Kotani, A. *Core Level Spectroscopy of Solids*; CRC Press: Boca Raton, FL, 2008; p 225.

(4) Gawelda, W.; Johnson, M.; de Groot, F. M. F.; Abela, R.; Bressler, C.; Chergui, M. *J. Am. Chem. Soc.* **2006**, *128*, 5001.
(5) Hu, Z.; von Lips, H.; Golden, M. S.; Fink, J.; Kaindl, G.; de Groot, F. M. F.; Ebbinghaus, S.; Reller, A. *Phys. Rev. B* **2000**, *61*, 5262.
(6) Kim, J. Y.; Hwang, S. H.; Kim, S. J.; Demazeau, G.; Choy, J. H.; Shimada, H. *J. Synchrotron Radiat.* **2001**, *8*, 722.
(7) Sham, T. K. *J. Am. Chem. Soc.* **1983**, *105*, 2269.
(8) Sugiura, C.; Kitamura, M.; Muramatsu, S. *J. Chem. Phys.* **1986**, *84*, 4824.
(9) Weaver, T. R.; Meyer, T. J.; Adeyemi, S. A.; Brown, G. M.; Eckberg, R. P.; Hatfield, W. E.; Johnson, E. C.; Murray, R. W.; Untereker, D. *J. Am. Chem. Soc.* **1975**, *97*, 3039.
(10) Hurst, J. K. *Coord. Chem. Rev.* **2005**, *249*, 313.
(11) Hurst, J. K.; Cape, J. L.; Clark, A. E.; Das, S.; Qin, C. Y. *Inorg. Chem.* **2008**, *47*, 1753.
(12) Liu, F.; Concepcion, J. J.; Jurss, J. W.; Cardolaccia, T.; Templeton, J. L.; Meyer, T. J. *Inorg. Chem.* **2008**, *47*, 1727.
(13) George, S. D.; Metz, M.; Szilagyi, R. K.; Wang, H. X.; Cramer, S. P.; Lu, Y.; Tolman, W. B.; Hedman, B.; Hodgson, K. O.; Solomon, E. I. *J. Am. Chem. Soc.* **2001**, *123*, 5757.
(14) Grush, M. M.; Chen, J.; Stemmler, T. L.; George, S. J.; Ralston, C. Y.; Stibrany, R. T.; Gelasco, A.; Christou, G.; Gorun, S. M.; PennerHahn, J. E.; Cramer, S. P. *J. Am. Chem. Soc.* **1996**, *118*, 65.
(15) Benfatto, M.; Della Longa, S.; Hatada, K.; Hayakawa, K.; Gawelda, W.; Bressler, C.; Chergui, M. *J. Phys. Chem. B* **2006**, *110*, 14035.
(16) Groot, F. d. *Coord. Chem. Rev.* **2005**, *249*, 31.
(17) Ankudinov, A. L.; Nesvizhskii, A. I.; Rehr, J. J. *Phys. Rev. B: Condens. Matter Mater. Phys.* **2003**, *67*, 115120.
(18) Rehr, J. J.; Albers, R. C. *Rev. Mod. Phys.* **2000**, *72*, 621.
(19) Rehr, J. J.; Ankudinov, A. L. *Coord. Chem. Rev.* **2005**, *249*, 131.
(20) Joly, Y. *Phys. Rev. B* **2001**, *63*, 125120.
(21) van der Laan, G.; Thole, B. T.; Sawatzky, G. A.; Verdaguer, M. *Phys. Rev. B* **1988**, *37*, 6587.
(22) Degroot, F. M. F.; Fuggle, J. C.; Thole, B. T.; Sawatzky, G. A. *Phys. Rev. B* **1990**, *42*, 5459.
(23) de Groot, F. M. F.; Hu, Z. W.; Lopez, M. F.; Kaindl, G.; Guillot, F.; Tronc, M. *J. Chem. Phys.* **1994**, *101*, 6570.
(24) Saes, M.; Bressler, C.; Abela, R.; Grolimund, D.; Johnson, S. L.; Heimann, P. A.; Chergui, M. *Phys. Rev. Lett.* **2003**, *90*, 047403.
(25) Hu, Z.; Golden, M. S.; Ebbinghaus, S. G.; Knupfer, M.; Fink, J.; de Groot, F. M. F.; Kaindl, G. *Chem. Phys.* **2002**, *282*, 451.
(26) Gilbert, J. A.; Eggleston, D. S.; Murphy, W. R.; Geselowitz, D. A.; Gersten, S. W.; Hodgson, D. J.; Meyer, T. J. *J. Am. Chem. Soc.* **1985**, *107*, 3855.
(27) Concepcion, J. J.; Jurss, J. W.; Norris, M. R.; Chen, Z. F.; Templeton, J. L.; Meyer, T. J. *Inorg. Chem.* **2010**, *49*, 1277.
(28) Sham, T. K. *J. Chem. Phys.* **1985**, *83*, 3222.
(29) Putilamantyla, P.; Ohno, M.; Graeffe, G. *J. Phys. B: At. Mol. Opt. Phys.* **1984**, *17*, 1735.
(30) Bressler, C.; Abela, R.; Chergui, M. *Z. Kristallogr.* **2008**, *223*, 307.
(31) de Siervo, A.; Landers, R.; de Castro, S. G. C.; Kleiman, G. G. *J. Electron Spectrosc. Relat. Phenom.* **1998**, *88*, 429.
(32) Guerra, C. F.; Snijders, J. G.; te Velde, G.; Baerends, E. J. *Theor. Chem. Acc.* **1998**, *99*, 391.
(33) Velde, G. T.; Bickelhaupt, F. M.; Baerends, E. J.; Guerra, C. F.; Van Gisbergen, S. J. A.; Snijders, J. G.; Ziegler, T. *J. Comput. Chem.* **2001**, *22*, 931.
(34) Van Lenthe, E.; Baerends, E. J. *J. Comput. Chem.* **2003**, *24*, 1142.
(35) Vosko, S. H.; Wilk, L.; Nusair, M. *Can. J. Phys.* **1980**, *58*, 1200.
(36) Perdew, J. P. *Phys. Rev. B* **1986**, *33*, 8822.
(37) Perdew, J. P.; Chevary, J. A.; Vosko, S. H.; Jackson, K. A.; Pederson, M. R.; Singh, D. J.; Fiolhais, C. *Phys. Rev. B* **1992**, *46*, 6671.
(38) Schipper, P. R. T.; Gritsenko, O. V.; van Gisbergen, S. J. A.; Baerends, E. J. *J. Chem. Phys.* **2000**, *112*, 1344.
(39) Staroverov, V. N.; Scuseria, G. E.; Tao, J. M.; Perdew, J. P. *J. Chem. Phys.* **2003**, *119*, 12129.
(40) Wang, F.; Ziegler, T. *Mol. Phys.* **2004**, *102*, 2585.
(41) Nilsson, A.; Martensson, N. *Phys. B* **1995**, *208*, 19.
(42) Shirley, E. L.; Soininen, J. A.; Rehr, J. J. *Phys. Scr.* **2005**, *T115*, 31.
(43) Nesvizhskii, A. I.; Rehr, J. J. *J. Synchrotron Radiat.* **1999**, *6*, 315.
(44) Kortboyer, S. W.; Grioni, M.; Speier, W.; Zeller, R.; Watson, L. M.; Gibson, M. T.; Schafers, F.; Fuggle, J. C. *J. Phys.: Condens. Matter* **1989**, *1*, 5981.
(45) Fronzoni, G.; Stener, M.; Decleva, P.; Wang, F.; Ziegler, T.; van Lenthe, E.; Baerends, E. J. *Chem. Phys. Lett.* **2005**, *416*, 56.
(46) Fronzoni, G.; Stener, M.; Decleva, P.; de Simone, M.; Coreno, M.; Franceschi, P.; Furlani, C.; Prince, K. C. *J. Phys. Chem. A* **2009**, *113*, 2914.
(47) Ogasawara, K.; Iwata, T.; Koyama, Y.; Ishii, T.; Tanaka, I.; Adachi, H. *Phys. Rev. B* **2001**, *64*, 115413.
(48) Ikeno, H.; Mizoguchi, T.; Tanaka, I. *Phys. Rev. B* **2011**, *83*, 155107.
(49) Batista, E. R.; Martin, R. L. *J. Am. Chem. Soc.* **2007**, *129*, 7224.
(50) Yang, X.; Baik, M. H. *J. Am. Chem. Soc.* **2006**, *128*, 7476.
(51) Daul, C.; Goursot, A. *Inorg. Chem.* **1985**, *24*, 3554.
(52) Stöhr, J. *NEXAFS Spectroscopy*; Springer-Verlag: Berlin, Heidelberg, New York, 1996.